Universitat Politècnica de Catalunya (UPC)
Universitat Autònoma de Barcelona (UAB)
Universitat de Barcelona (UB)
Institut de Ciències Fotòniques (ICFO)

http://www.photonicsbcn.eu

Master in Photonics

MASTER THESIS WORK

Ultracold dipolar bosons trapped in atomtronic circuits

Marc Rovirola Metcalfe

Supervised by Dr. Montserrat Guilleumas, (UB)
and Dr. Bruno Juliá-Díaz, (UB)

Presented on date 19th July 2022

Registered at

Escola Tècnica Superior d'Enginyeria de Telecomunicació de Barcelona

Ultracold dipolar bosons trapped in atomtronic circuits

Marc Rovirola Metcalfe
Advisors: Montserrat Guilleumas and Bruno Juliá-Díaz

Departament de Física Quàntica i Astrofísica, Facultat de Física, Universitat de Barcelona, Martí i Franquès 1, 08028-Barcelona

E-mail: marc.rovirola@estudiantat.upc.edu

Abstract. We consider a ring-shaped triple-well potential with few polar bosons characterized by a long-range and anisotropic interaction. By diagonalizing the extended Bose-Hubbard Hamiltonian, that treats sites as macroscopic dipoles, we investigate the ground state properties of the system as we rotate the dipole angle and vary the on-site interaction strength. We find that the competition between dipole and on-site interaction lead to different ground states and that the entanglement between sites depends on the filling factor which can be fractional or integer, and whether the number of particles is odd or even. We further characterize the system by studying the condensed fraction and coherence properties.

Keywords: atomtronics, extended Bose-Hubbard, optical lattices

1 Introduction

Bose-Einstein Condensates (BECs) were first theorized in the 1920's but it was not until 1995 that it was achieved experimentally [1]. BEC is a state of matter exhibited by ultracold bosons, which is characterized by a macroscopic occupation of a single particle state. Thus, BECs manifest quantum properties in a macroscopic scale. Further experimental breakthroughs have allowed longer time scales and better spatial resolution enabling trapping of atoms in different geometries. Studies from the recent years have shown that BEC properties can be exploited for quantum technologies, such as, entanglement manipulation [2], transistor-like properties [3, 4] and persistent currents [5]. The atomtronics field studies these quantum phenomena and capitalizes on them to develop quantum devices [6].

To create ultracold quantum gases, atoms are loaded into potential wells created by magnetic confinement or optical lattices. The latter are created by an array of lasers which can produce set-ups with many different shapes and potential strengths that will heavily influence the properties of the system [7]. Triple-well potentials have gained interest due to their simplicity but rich phenomenology [8–10]. Two types of set-up are attainable: fully connected wells in a triangular shape or one-dimensional aligned wells. The former being the smallest system to include angular momentum with a superfluid phase that is manifested with vortex currents [11].

Recent experimental techniques have allowed trapping of polar atoms, such as Erbium [12] and Chromium [13, 14] displaying strong dipole-dipole interaction. A major feature for using

polar atoms is the long range and anisotropic behaviour of the interaction leading to new phase transitions [15] and fragmentation [16]. Studies with polar atoms in triple-well potentials introduce phenomena as Josephson-like dynamics [17] for one-dimensional aligned wells and self-trapping [18] in ring-shaped potential wells.

In this work we consider few bosons trapped in a ring-shaped triple-well potential at zero temperature. The static properties of the system are described with an extended Bose-Hubbard Hamiltonian that includes nearest-neighbour tunneling, on-site interaction and long range dipole-dipole interaction. Through exact diagonalization we compute the ground state properties varying the on-site interaction strength and the dipole direction and determine how the number of particles affects the correlation between sites, average occupation, condensed fraction and entanglement spectrum.

This work is organized as follows: Section 2 introduces the effect of the dipole interaction and the extended Bose-Hubbard Hamiltonian. Section 3 recalls the many-body properties used to characterize the system. Section 4 shows the ground state properties of the Hamiltonian with varying parameters. Finally, Section 5 presents the conclusions.

2 Dipolar Bose-Hubbard Hamiltonian

The potential-wells (or sites) are located in an equilateral triangle and the atoms are loaded with the same polarization direction. The ratio between the number of particles, N, and wells, M is called filling factor, $\nu = N/M$. We consider an effective dipole, $\mathbf{d}$ for each site [15, 19–21]. The dipole interaction is written in the following form:

$$V_{dd;i,j} = C_{dd}\,\frac{1-3\cos^2(\theta_{d;ij})}{|\mathbf{r}_i-\mathbf{r}_j|^3}\,, \tag{1}$$

where $i,j=1,2,3$ represent the site indexes, and $\mathbf{r}_i$ is the position of each well as shown in Figure 1 (a), C_{dd} is the strength of the dipole interaction, and $\theta_{d;ij}$ is the angle between the dipole direction and the vector $\mathbf{r}_{ij} \equiv \mathbf{r}_i - \mathbf{r}_j$. Due to the geometry, the distance between wells is the same with $|\mathbf{r}_i - \mathbf{r}_j| = 1$ in dimensionless units.

Adding this term we extend the Bose-Hubbard model which only considers tunneling (J) and on-site interaction (U). With this framework, we are able to compute the ground state of the system and calculate its properties such as degree of condensation, entropy and the probability density of each state. Ultimately, the extended Bose-Hubbard is

$$H = -J\sum_{<i,j>}^{3}\hat{a}_i^\dagger\hat{a}_j + h.c. + \frac{U}{2}\sum_{i}^{3}\hat{n}_i(\hat{n}_i-1) + \sum_{\substack{i,j\\ i\neq j}}^{3} V_{dd;i,j}\,\hat{n}_i\hat{n}_j\,, \tag{2}$$

where the first term is the tunneling between neighboring wells with $\hat{a}_i, \hat{a}_i^\dagger$ being the bosonic annihilation and creation operators, respectively. The second term represents the on-site interaction and counts the number of pairs that can be formed in a single well, where $\hat{n}_i = \hat{a}_i^\dagger\hat{a}_i$ is the number operator and counts the number of atoms. The last term is the extension to the model that includes the dipole interaction described previously.

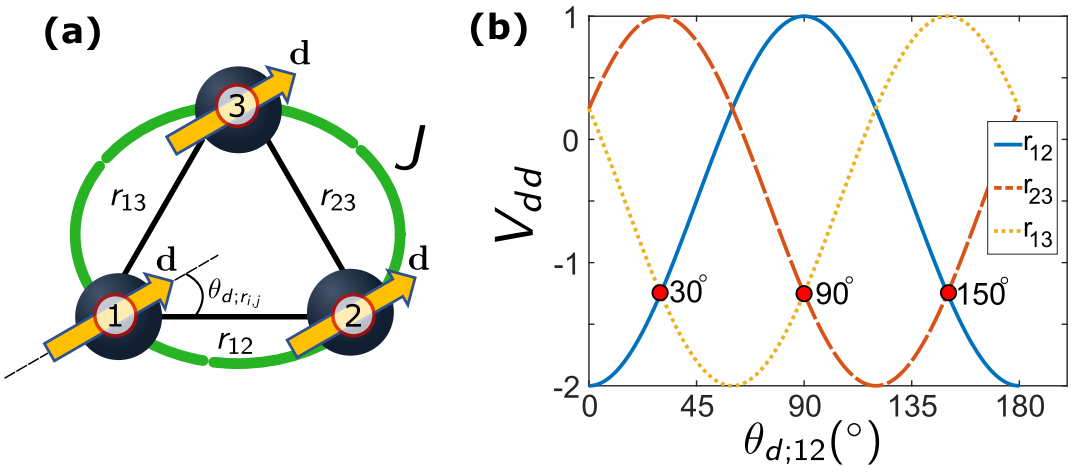

Figure 1: **(a)** Schematic representation of the triple well set-up in an equilateral shape with each site labeled. The yellow arrows represent the macroscopic dipole, **d**, of each well, the green dashed line represents the tunneling with strength J and $\theta_{d;ij}$ is the angle between the dipole direction and the vector $\mathbf{r}_{ij}$. **(b)** Representation of Equation (1) with $C_{dd} = 1$ as a function of the dipole angle $\theta_{d;12}$, where $\theta_{d;23} = \theta_{d;12} + 60°$ and $\theta_{d;13} = \theta_{d;12} + 120°$.

It is convenient to work with Fock states which describe the distribution of particles amongst the three wells. The bosonic wavefunction can be written as a superposition of Fock states as

$$|\Psi\rangle = \sum_{n_1,n_2,n_3=0}^{N} C_{n_1,n_2,n_3} |n_1 n_2 n_3\rangle \ , \tag{3}$$

where $n_i = 0, 1, ..., N$ is the number of atoms in site i and $|C_{n_1,n_2,n_3}|^2$ is the probability of the corresponding Fock state $|n_1 n_2 n_3\rangle$. The Fock basis of the Hamiltonian is the combination of Fock states that contain N atoms distributed in M wells and has a dimension $D = \frac{(N+M-1)!}{N!(M-1)!}$. Applying the basis to Equation (2) outputs a $D \times D$ matrix which can be solved using exact diagonalization to find the eigenenergies and eigenstates of the Hamiltonian.

To further understand the effect of the dipole interaction, a plot of $V_{dd;i,j}$ as a function of the dipole direction is shown in Figure 1 for all site pairs. The three red points mark the crossing of two curves. At these points the interaction between 2 pairs of sites are attractive with the same strength, crossing these points by varying the dipole angle $\theta_{d;ij}$ changes the sites that lower the energy.

3 Quantum many-body properties

3.1 Ground state probability

In order to characterize the system, we first obtain the many-body ground state of the system, $|\Psi_{GS}\rangle$, in the Fock basis. The probability of finding the system in a particular Fock state $|n_1 n_2 n_3\rangle$ is given by $|C_{n_1,n_2,n_3}|^2 = |\langle n_1 n_2 n_3 | \Psi_{GS}\rangle|^2$. Figure 2 compares the ground state probabilities of a commensurate system ($\nu = 1$) with and without dipole interaction when the atoms are polarized in the $\mathbf{r}_{12}$ direction. Figure 1 (b) shows that sites 1-2 have attractive interaction with strength -2,

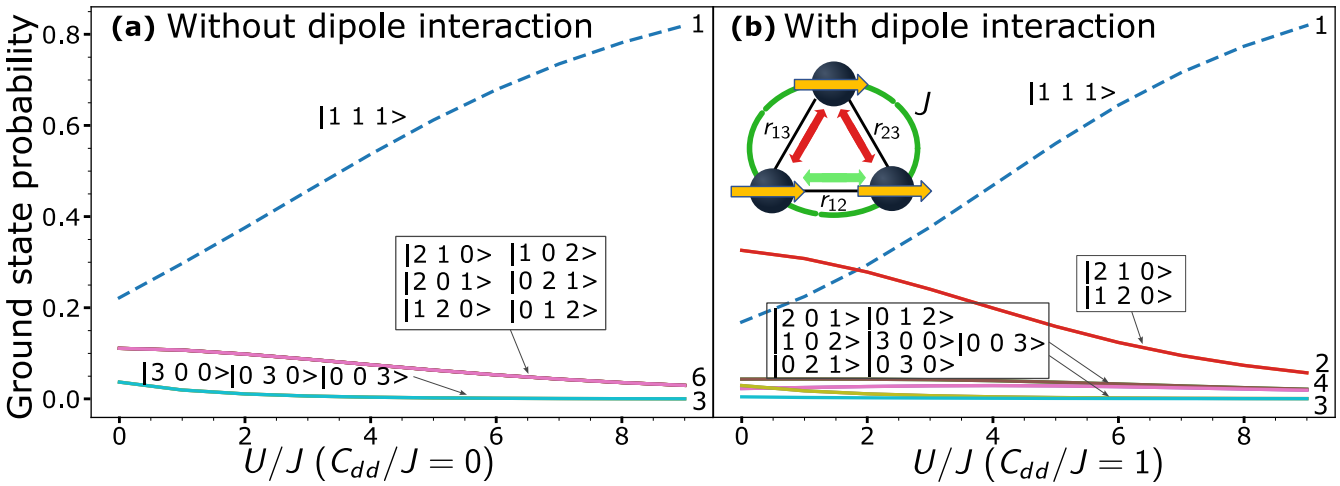

Figure 2: Probabilities $|C_{n_1,n_2,n_3}|^2$ associated to the many-body ground state **(a)** without having dipole interaction and **(b)** having dipole interaction when all atoms are polarized in the $\mathbf{r}_{12}$ direction with $C_{dd}/J = 1$. The inset in **(b)** represents the set-up where the green arrow illustrates attractive interaction between site 1 and 2, while the red arrow illustrates repulsion between sites 1 and 3, and 2 and 3. The Fock state that each line represents is indicated above it and the numbers at the end of each line illustrates the degeneration the line depicts.

while 1-3 and 2-3 are repulsive with strength 0.25. The dipole interaction gives a higher probability to the states $|210\rangle$ and $|120\rangle$ (degenerate energy) than the rest due to the attractive interaction. As the on-site interaction increases the system will minimize the number of pairs to lower its energy. When the on-site interaction energy dominates the dipole interaction, the bosons will separate equally in each well in a Mott-like state $|\Psi\rangle = |N/3, N/3, N/3\rangle$. This can be seen with the dashed-line in both panels in Figure 2.

3.2 Degree of condensation

At absolute zero and in absence of interactions the atoms of a bosonic gas populate a single-particle state. Interactions, such as on-site, can remove particles from the condensate into other states. This can deplete a fraction of the condensate, or if the interaction is large enough it can even fragment it. By using the one-body density matrix and applying it to our ground state we can calculate the condensed fraction (largest eigenvalue) of our system as we vary parameters, such as, dipole orientation and on-site strength. The one-body density matrix operator associated to the ground state is:

$$\hat{\rho}_{i,j} = \frac{1}{N} \langle \Psi_{GS} | \hat{a}_i^\dagger \hat{a}_j | \Psi_{GS} \rangle . \tag{4}$$

The eigenvalues, p_i, of the one-body density matrix represent the relative occupation of the corresponding eigenstate, where $p_1 + p_2 + p_3 = 1$ and $p_1 > p_2 > p_3$. For a singly condensed system $p_1 \approx 1$ while $p_2, p_3 \approx 0$. On the contrary, for a fragmented system, two or more eigenvalues will be comparable. The eigenvectors of the one-body density matrix are the so-called natural orbits or single-particle states.

3.3 Entanglement

The crossing of states in the ground state probabilities indicates that there are correlations between sites which can be quantified with the von Neumann entropy [18, 22]. The correlations can be obtained by calculating the reduced density matrix of one site, that is, splitting the system in two parts and tracing out one of them. In our system there are three possible bipartite splittings: (1,23), (2,13) or (3,12). Since the number of particles is conserved, we can define any Fock state as:

$$|n_1, n_2, N - n_1 - n_2\rangle = |n_1\rangle \otimes |n_2\rangle \otimes |N - n_1 - n_2\rangle .$$

Tracing out sites 2 and 3 leaves us with the reduced density matrix of site 1:

$$\rho_1 = \mathrm{Tr}_{23}(\rho) = \sum_{n_2, N-n_1-n_2} \langle n_2, N - n_1 - n_2| \left(|\Psi_{\mathrm{GS}}\rangle \langle \Psi_{\mathrm{GS}}|\right) |n_2, N - n_1 - n_2\rangle = \sum_{n_1} \lambda_{n_1} |n_1\rangle \langle n_1| , \tag{5}$$

where λ_{n_1} are the Schmidt coefficients which satisfy $\sum_{n_1} \lambda_{n_1} = 1$. The difference between the two largest Schmidt coefficients is called the Schmidt gap ($\Delta\lambda$) and is a good measure to determine phase and ground state transitions [22].

With the reduced density matrix, the von Neumann entropy can be calculated as follows:

$$S_i = -\,\mathrm{Tr}(\rho_i \log \rho_i). \tag{6}$$

As the partial density matrix is diagonal, the von Neumann entropy can be written as $S = -\sum \lambda_{n_i} \log \lambda_{n_i}$. If the subsystems exhibit entanglement, entropy is maximized with equal Schmidt coefficients, $\Delta\lambda = 0$. On the contrary, if the subsystems are uncorrelated, only one non-zero Schmidt coefficient exists, resulting in zero entropy.

3.4 Average occupation

Due to the effect of the dipole interaction, the density of particles in each site will depend on the type of interaction, i.e., attractive or repulsive. In the strong dipole interaction limit ($C_{dd} \gg U, J$), the number of particles in the repulsive site is zero while the dipole-attractive sites will distribute the particles as evenly as possible. This can be calculated with the average occupation, $\langle n_i \rangle$, over the ground state.

4 Ground state properties

4.1 Mott-like transition in the zero-tunneling limit, and $\nu \in Z^+$

Setting tunneling to zero, $J = 0$, an analytical solution can be found of the Hamiltonian since the on-site and dipole interaction coefficients lie in the diagonal. In the case of integer filling factors, we can determine at which U the transition into a Mott-like state as shown in Figure 2 occurs as we rotate the dipole angle by comparing the energy of the Mott-like state and the dipole-favored states. The energy of theses states is calculated with the Hamiltonian:

$$E_{|N-n_i,n_i,0\rangle} = \frac{U}{2}[(N - n_i)^2 + n_i^2 - N] + C_{dd}[1 - 3\cos^2(\theta_{d;ij})](Nn_i - n_i^2).$$

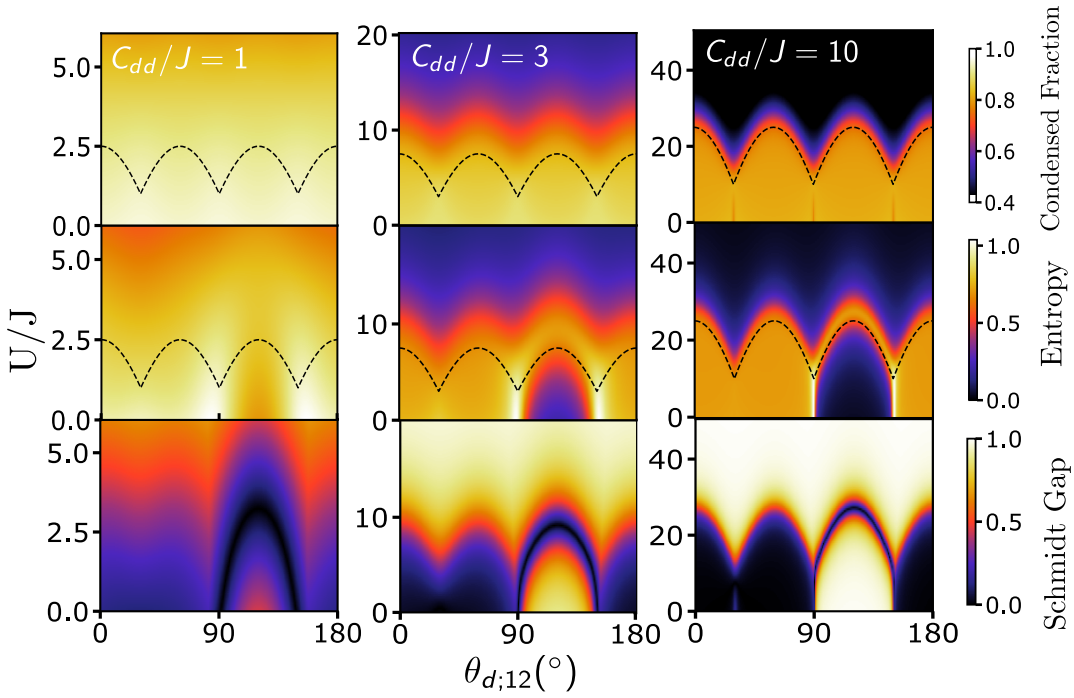

Figure 3: Results for $\nu = 1$ with each column representing different dipole strengths, from left to right $C_{dd}/J = 1, 3, 10$. The top row shows the condensed fraction (largest eigenvalue of the one-body density matrix). The middle row shows the von Neumann entropy of ρ_1 (tracing sites 2 and 3) as a function of U/J and the dipole direction. The bottom row shows the Schmidt gap of ρ_1 as a function of U/J and the dipole direction. The dashed black lines represent the values of U_c where the ground state transition occurs in the zero-tunneling limit, Equation (7).

$$E_{|\frac{N}{3}\frac{N}{3}\frac{N}{3}\rangle} = \sum_{\substack{i,j \\ i\neq j}}^{3} (1 - 3\cos^2(\theta_{d;ij})) \cdot \hat{n}_i \hat{n}_j =$$

$$\frac{N}{3}[1 - 3\cos^2(\theta_{d;12}) + 1 - 3\cos^2(\theta_{d;12} + 60^\circ) + 1 - 3\cos^2(\theta_{d;12} + 120^\circ)] = -N/2\,.$$

By imposing the two energies to be equal, it yields the critical U at which the transition occurs

$$U_c(\theta_{d;ij}) = \frac{-N - 2 \cdot C_{dd}[1 - 3\cos^2(\theta_{d;ij})](Nn_i - n_i^2)}{[(N - n_i)^2 + n_i^2 - N]}\,, \tag{7}$$

with i and j being the dipole-favored sites. At the thermodynamic limit ($N \to \infty$) and using the following approximations: $n_i \approx N/2$ and $N/2 \gg 1$, the critical U_c at which the transition occurs only depends on the dipole strength and orientation:

$$U_c^{N\to\infty}(\theta_{d;ij}) = C_{dd}[1 - 3\cos^2(\theta_{d;ij})]\,. \tag{8}$$

4.2 Dipole strength effect

Interesting effects from the dipole interaction start with $N = 3$. Figure 3 shows the effect of the dipole strength on the condensed fraction, entropy, and Schmidt gap. As the dipole

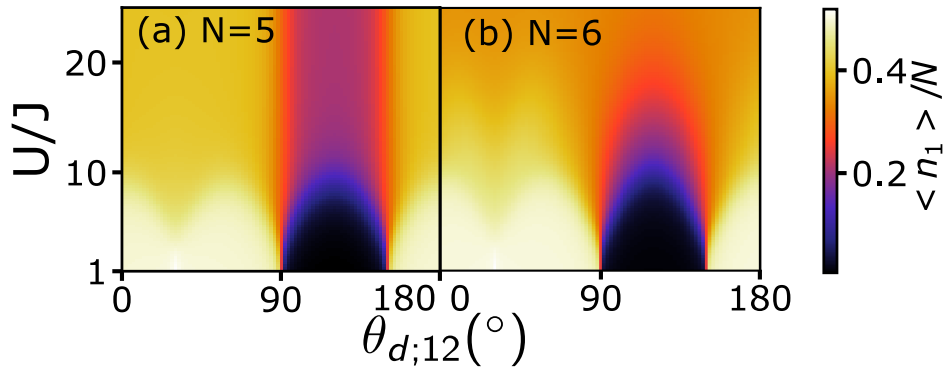

Figure 4: Normalized average occupation of site 1, $\langle n_1 \rangle / N$, as a function of U/J and dipole direction with $C_{dd}/J = 3$ for **(a)** $N = 5$ and **(b)** $N = 6$.

strength increases (from left to right panel), the on-site repulsion strength needed to separate pairs of particles will increase and the ground state transitions are more abrupt. For large dipole interaction, the black-dashed line represents U_c from Equation (7), above which the condensed fraction decreases, highlighting the ground state transition, e.g., from a superposition of states $|210\rangle + |120\rangle$ to a Mott-like state $|111\rangle$. It should be noted that the eigenvectors change with the dipole angle. For small dipole strengths and in a non-interacting case ($U/J = 0$), all particles are part of the condensate with $p_1 \approx 1$. As the on-site interaction increases there is a depletion of the condensate and at the limit of a very large repulsion ($U/J \gg 1$) the system becomes fragmented with three single-particle states with the relative occupation values converging to 1/3. For all dipole strengths and $U < U_c(\theta_{d;ij})$ there is a macroscopical condensed fraction showing that the dipole interaction favors the condensed state which may be crucial for atomtronic circuits.

Regarding the correlation between sites, Figure 3 (second and third row) shows the von Neumann entropy and Schmidt gap tracing out sites 2-3, that is having the correlation between site 1 and subsystem 2-3 (1,23). A strong correlation is obtained between the subsystems in the dipole-dominating range demonstrated by the near-zero Schmidt gap and high entropy. Moreover, a sudden drop in both values appears from 90 to 150 degrees. This can be understood with Figure 1 (b), since between those angles, site 1 is repulsive with sites 2 and 3 breaking the correlation between the subsystems. Due to the geometry there is rotational symmetry and therefore, the results shown for this subsystem are equivalent to (3,12) and (2,13) just shifted 60 and -60 degrees respectively.

4.3 Average occupation

As explained in Section 3.4, in the dipole dominating range and in the dipole angles where the site is repulsive, the average occupation tends to zero while the remaining sites host the particles equally with a normalized average occupation of 1/2. This is reflected for site 1 in Figure 4 with the dark region between 90 an 150 degrees and the light regions at all other angles. At the limit of large on-site interaction ($U \gg C_{dd}, J$) the particles tend to distribute equally between sites to minimize the number of pairs. Two cases arise: (i) non-commensurate number of particles where the favored sites have larger occupation values than the repulsive as seen in Figure 4 (a). (ii)

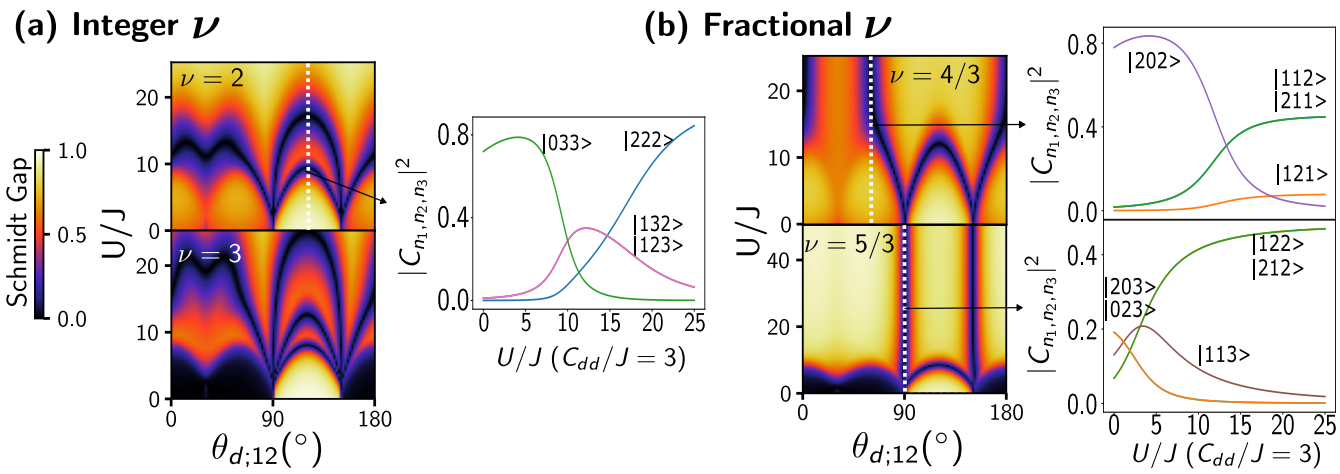

Figure 5: Schmidt gap as a function of U/J and the dipole angle with a dipole strength of $C_{dd}/J = 3$ for two different filling factors: **(a)** For integer $\nu = 2, 3$ as indicated. **(b)** For fractional $\nu = 4/3, 5/3$ as indicated. The white-dashed lines show the vertical cuts at which the ground state probabilities are shown for single dipole orientations. Only relevant states are shown in the ground state probabilities as a function of U/J.

Commensurate number of particles where all sites have an average occupation value of 1/3 as seen in Figure 4 (b). At intermediate values of U and larger N there will be changes in the average occupation as the on-site interaction increases and it minimizes particle pairs until it reaches to its minimum energy state. For example, for incommensurate particle number, $N = 8$, as U increases, different ground states are obtained: $|440\rangle \rightarrow |431\rangle + |341\rangle \rightarrow |332\rangle$. At every transition the average occupancy decreases until it reaches the Mott-like state. Also, the results show that by manipulating the dipole orientation we can modify at will the population density of the system in the dipole-dominating range.

4.4 Entanglement Spectrum

To characterize the entanglement spectrum the Schmidt gap is used as defined in Section 3.3. It should be emphasized that due to the geometry of our system the sites are symmetrical with respect to 60 degree rotations; therefore the effects shown for subsystem (1,23) will be shifted 60 degrees for the subsystem (3,12) and -60 degrees for subsystem (2,13).

As a result of the dipole interaction the entanglement varies depending on the filling factor and whether the number of particles is odd or even. At the limit of large dipole interaction ($C_{dd} \gg J, U$) the particles will be distributed amongst the dipole-attractive sites, as seen in the ground state probabilities in Figure 5 for $\nu = 2, 4/3$. These wavefunctions can be expressed as a product of states displaying no entanglement and a Schmidt gap close to 1. On the other hand, if the particles cannot be distributed equally, the system will be in a superposition of states with the extra particle being shared between the dipole-favored sites with a wavefunction that cannot be expressed as a product of states. The superposition of states displays large correlations between subsystems in the dipole angles where the studied site has attractive interaction, as seen in Figure 5 for $\nu = 3, 5/3$.

Furthermore, Figure 5 (a) and (b) displays vertical cuts at fixed dipole orientations represented with white dashed-lines that show the corresponding state probabilities, $|C_{n_1,n_2,n_3}|^2$, of the ground state. Whenever the highest probability states cross, the Schmidt gap drops to 0 showing strong correlation between sites. Additionally, fractional filling factors can exhibit entanglement between sites regardless of on-site interaction at certain dipole angles. That is because the ground state at these angles is a superposition which cannot be a expressed as a product of states.

5 Conclusions

We have shown that triple-well potentials loaded with polar atoms show very rich phenomena and strongly depend on the interaction strengths, number of particles and dipole orientation. We showed that the crossing in the ground states is directly linked to correlations between sites and that entanglement for incommensurate filling can be sustained regardless of the on-site interaction for certain dipole orientations. We give an analytic expression to find the on-site strength at which the systems evolves into a Mott-like state, and show that above this value the condensate gets depleted or fragmented. Furthermore, we found that contrary to on-site interaction, dipole interactions maintain the condensed state with little depletion in the studied dipole strengths. Moreover, we have shown that the orientation of the dipoles can be used as a source for entanglement manipulation which could be the ground for future studies. Further studies can be carried out, such as, vortex currents in ring-shaped potentials which have recently been proven experimentally [23], ground state and transport properties of two triple-well rings with different tunneling connections and geometries and larger dimensional systems.

Acknowledgments

I would like to thank my tutors Montserrat Guilleumas and Bruno Juliá-Díaz for the opportunity, encouragement, time investment and support throughout these months to complete this project.

References

[1] M. H. Anderson, J. R. Ensher, M. R. Matthews, C. E. Wieman, and E. A. Cornell, Science **269**, 198 (1995).
[2] M. Fadel, T. Zibold, B. Décamps, and P. Treutlein, Science **360**, 409 (2018).
[3] A. Micheli, A. J. Daley, D. Jaksch, and P. Zoller, Phys. Rev. Lett. **93**, 140408 (2004).
[4] Z. Zhang, V. Dunjko, and M. Olshanii, New J. Phys. **17**, 125008 (2015).
[5] T. F. Viscondi and K. Furuya, J. Phys. A: Math. Theor. **44**, 175301 (2011).
[6] L. Amico et al., AVS Quantum Sci. **3**, 039201 (2021).
[7] S. Giovanazzi, A. Görlitz, and T. Pfau, Phys. Rev. Lett. **89**, 130401 (2002).
[8] S. K. Haldar and O. E. Alon, J. Phys.: Conf. Ser **1206**, 012010 (2019).
[9] K. W. W., E. R. Castro, A. Foerster, and L. F. Santos, Phys. Rev. E **105** (2022).
[10] C. Lushuai, I. Brouzos, S. Zöllner, and P. Schmelcher, New J. Phys. **13**, 033032 (2011).
[11] G. Arwas, A. Vardi, and D. Cohen, Phys. Rev. A **89** (2014).
[12] K. Aikawa et al., Phys. Rev. Lett. **108**, 210401 (2012).
[13] T. Lahaye et al., Phys. Rev. Lett. **101**, 080401 (2008).
[14] B. Pasquiou et al., Phys. Rev. Lett. **106**, 015301 (2011).
[15] A. Gallemí, M. Guilleumas, R. Mayol, and A. Sanpera, Phys. Rev. A **88**, 063645 (2013).

[16] H. Lu and Y. I. Su, Sci China-Phys Mech Astron **55**, 1535 (2012).
[17] T. Lahaye, T. Pfau, and L. Santos, Phys. Rev. Lett. **104**, 170404 (2010).
[18] L. Dell'Anna, G. Mazzarella, V. Penna, and L. Salasnich, Phys. Rev. A **87**, 053620 (2013).
[19] H.-K. Wu and W.-L. Tu, Phys. Rev. A **102**, 053306 (2020).
[20] T. Lahaye, T. Pfau, and L. Santos, Phys. Rev. Lett. **104**, 170404 (2010).
[21] A. Safavi-Naini, Ş. G. Söyler, G. Pupillo, H. R. Sadeghpour, and B. Capogrosso-Sansone, New J. Phys. **15**, 013036 (2013).
[22] A. Gallemí et al., New J. Phys. **17**, 073014 (2015).
[23] L. Klaus et al., arXiv e-prints , arXiv:2206.12265 (2022).